Editors' Suggestion

High-Purity Generation and Switching of Twisted Single Photons

Haoqi Zhao,[1,2,*] Yichen Ma,[3,4,*] Zihe Gao,[2] Na Liu,[3,4] Tianwei Wu,[2] Shuang Wu,[2] Xilin Feng,[1] James Hone,[5] Stefan Strauf,[3,4,†] and Liang Feng[2,1,‡]

[1]*Department of Electrical and Systems Engineering, University of Pennsylvania, Philadelphia, Pennsylvania 19104, USA*
[2]*Department of Materials Science and Engineering, University of Pennsylvania, Philadelphia, Pennsylvania 19104, USA*
[3]*Department of Physics, Stevens Institute of Technology, Hoboken, New Jersey 07030, USA*
[4]*Center for Quantum Science and Engineering, Stevens Institute of Technology, Hoboken, New Jersey 07030, USA*
[5]*Department of Mechanical Engineering, Columbia University, New York, New York 10027, USA*

(Received 1 February 2023; accepted 5 October 2023; published 31 October 2023)

Quantum technologies, if scaled into a high-dimensional Hilbert space, can dramatically enhance connection capabilities with supporting higher bit rates and ultrasecure information transfer. Twisted single photons, carrying orbital angular momentum (OAM) as an unbounded dimension, could address the growing demand for high-dimensional quantum information encoding and transmission. By hybrid integration of two-dimensional semiconductor WSe_2 with a spin-orbit-coupled microring resonator, we demonstrate an integrated tunable twisted single photon source with the ability to precisely define and switch between highly pure spin-OAM states. Our results feature a single photon purity of $g^{(2)}(0) \sim 0.13$ with a cavity-enhanced quantum yield of 76% and a high OAM mode purity up to 96.9%. Moreover, the demonstrated quantum-chiral control can also enable new quantum functionality such as single photon routing for efficient quantum information processing on chip.

DOI: 10.1103/PhysRevLett.131.183801

Single photons, as a fundamental carrier of information, are widely used to transmit quantum information that can be simultaneously encoded on multiple degrees of freedom (DOFs), including polarization, phase, frequency, time, and path [1–4]. Polarizations (i.e., photon spins), as the most extensively studied DOF, construct a two-dimensional (2D) space to realize a qubit as a coherent superposition of two orthogonal polarization states. In contrast, twisted single photons, in the form of twisted phase fronts, can carry a number of different OAM states. In this scenario, discrete topological charges of $l\hbar$ associated with twisted single photons, where l is an unbounded integer corresponding to the OAM order, can yield a high-dimensional Hilbert space to create a qudit [5]. This unique property not only allows higher quantum channel capacity beyond one bit per photon, but also offers enhanced security against eavesdropping and quantum cloning [6–11], leading to high-dimensional quantum key distribution [7,10], high-dimensional quantum entanglement [12], and multi-DOF quantum teleportation [13].

To construct high-dimensional quantum transmission links, it is critical to first develop a strategy for the efficient generation and manipulation of twisted single photons carrying high-purity OAMs with high fidelity. However, current demonstrations are mainly based on the free space spatial light modulation of single photons generated by spontaneous parametric down-conversion, which is non-deterministic and inefficient with low brightness [14,15]. Hybrid integration of solid-state quantum emitters into photonic integrated circuits provides a solution to efficient, deterministic single photon sources with high quantum yield for on-chip quantum photonic technologies [16]. In parallel, judiciously designed on-chip photonic structures facilitate phase front shaping of single photons, directly enabling an integrated quantum-chiral interface to create single photon OAM states on demand [17]. Nevertheless, recent attempts on on-chip twisted single photon emitters are limited to fixed OAM superposition states with relatively low fidelity and also lack reconfigurability [18–20]. The high-purity generation and switching between different pure OAM states on a single photon level require on-chip breaking of the time reversal symmetry together with delicate spin-orbit chiral control, which still remains a grand challenge on on-chip quantum photonic platforms.

Here, we overcome this fundamental limitation and demonstrate the first on-chip tunable twisted single photon source which is tailored to support a pair of coupled quantum-chiral interfaces for the spin-orbit chiral control in the quantum regime. Specifically, the device consists of a dielectric microring resonator made of Si_3N_4, coupled with a monolayer of the 2D semiconductor WSe_2, for the high-purity generation and magnetic switching of twisted single photons between different pure OAM states with opposite topological charges (Fig. 1). The spin-orbit chiral control arises from the microring resonator with the strategically designed dimensions of its cross-section. With the optimized geometrical parameters, the whispering gallery modes supported in the microring possess equal-amplitude

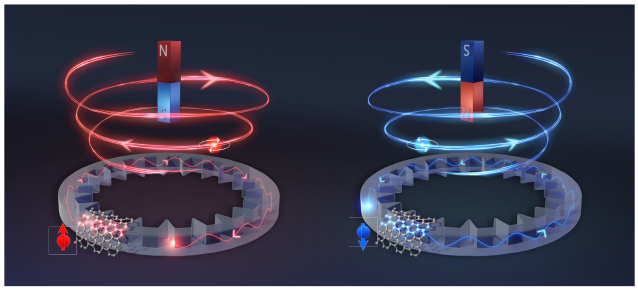

FIG. 1. Schematic of an on-chip switchable twisted single photon source. By hybrid integration of monolayer WSe_2, a magnetic-tuned single-spin quantum emitter is formed on a microring resonator that features a pair of quantum-chiral interfaces at the outer and inner sidewalls. When tuned on resonance, the quantum emitter at the outer sidewall emits single photons into one of the chiral modes in the microring, which are subsequently coupled out by the angular grating inscribed at the inner sidewall, emitting twisted single photons in free space. Under an external magnetic field pointing upward at the sample plane (left), the intrinsic spin of quantum emission is σ_+, which excites only the CW mode in the microring. Consequently, the emitted twisted single photons carry a photon spin of σ_- with an OAM topological charge of $+l$. If the magnetic field is switched downward (right), all the chiral signatures are reversed. Intrinsic σ_--polarized quantum emission excites only the CCW mode, which leads to radiations of σ_+-polarized twisted single photons with an OAM topological charge of $-l$.

out-of-phase radial and azimuthal polarization components at the sidewalls, so pure transverse spins (i.e., circularly polarized field) emerge there. The transverse spins consequently feature a spin-orbit-locking mechanism [21–23], which defines the polarization of the clockwise (CW) or counterclockwise (CCW) mode to be spin-up (σ_+) or spin-down (σ_-) at the outer sidewall while the spin directions reverse at the inner sidewall, thereby forming two coupled quantum-chiral interfaces (see Supplemental Material [24]). At the quantum-chiral interface, a chiral quantum emitter with a spin-dependent optical transition selectively excites either CW or CCW mode according to the designed spin-orbit locking [32]. Note that, in this scenario, the breaking of the time reversal symmetry of the quantum emitter by an external magnetic field is translated into the breaking of the chiral symmetry of the microring to facilitate the spin-orbit chiral control required for the switching of twisted single photons. However, it is technically difficult to precisely place a chiral quantum emitter at one of the quantum-chiral interfaces because of the nature of most solid-state quantum emitters being randomly distributed in terms of locations. While recent studies have achieved the precise localization of single quantum dots with an average position uncertainty of 10 nm [33], these methods require complicated positioning and alignment techniques. In contrast, we use a self-aligned method by exploiting the strain-induced quantum emitter in a monolayer of WSe_2 on top of the Si_3N_4 microring: the mechanical strain inherently arising from the three-dimensional (3D) geometry of the microring forms a local stressor hosting zero-dimensional (0D) excitons in WSe_2 at the outer sidewall of the microring, assuring the desired quantum-chiral coupling in a deterministic manner [27,31,34–37]. It is also worth noting that the device itself carries rotational symmetry that assures that the azimuthal position of the quantum emitter does not affect the mode inside the ring resonator and the spin-OAM state. As a result, there is no need for any specific azimuthal control of positioning the quantum emitter in our experiment.

With the selected intrinsic exciton emission blue detuned from the cavity resonance, the magnetic tuning of optical transition associated with the exciton in WSe_2 ensures that only one spin branch is tuned on resonance with the cavity at a time to define and switch the chirality of the quantum emitter. With on-resonance σ_+ optical transitions occurring at the outer sidewall of the microring, quantum light emission is enforced to efficiently couple to only the TE-polarized CW mode. The angular grating inscribed on the inner sidewall converts the guided CW mode into free space twisted single photon emission in the form of a σ_--polarized Bessel beam in the far field [38], with respect to the following phase matching condition: $l = N - M + 1$, where l is the topological charge of the pure OAM state, N is the resonant order of the whispering gallery mode in the microring, and M is the number of scatterers in the angular grating. The switching of the magnetic field facilitates the spin-orbit chiral control: it flips the spin of optical transitions from σ_+ to σ_- at the outer sidewall and thus the power flow from CW to CCW in the microring, conveniently reversing the chiral features of a twisted single photon to spin-up polarization σ_+ and a topological charge of $-l$.

A Si_3N_4 microring resonator coupled with a bus waveguide was fabricated on a SiO_2 substrate using electron beam lithography, followed by hybrid integration of monolayer WSe_2 [Fig. 2(a)]. Here, the inner radius of the microring is 7.25 μm, and the dimensions of its cross-section are 500 nm × 220 nm to support transverse spins at sidewalls for the fundamental TE mode. Two grating couplers with the periodicity of 490 nm and the filling factor of 0.45 were also fabricated on both sides of the bus waveguide to illustrate the power flow direction inside the microring. To characterize the strain-induced quantum emitter in WSe_2 and its coupling with the microring resonator, we pumped the quantum emitter using a laser diode at the wavelength of 635 nm and measured the magnetic field-dependent spectrum of its spontaneous emission at a temperature of 4 K [Fig. 2(b)]. Under an external magnetic field, the degeneracy of σ_+ and σ_- branches of the emission becomes lifted [25]. Note that for the studied quantum emitter, the low-energy branch dominates over the high-energy one because of anisotropic strain and thermalization effects, thereby resulting in

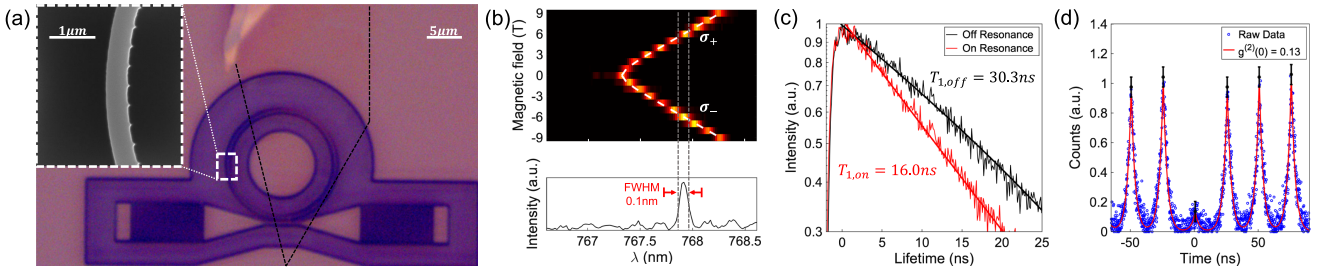

FIG. 2. Characterization of quantum light emission. (a) Optical microscope image of the device: a microring coupled with a bus waveguide connected with two grating couplers fabricated on a Si_3N_4-on-SiO_2 platform. A monolayer WSe_2 flake is transferred on top to form the quantum emitter on the ring, marked by the black dotted line. Inset shows the scanning electron microscope graph of the microring resonator where equidistant scatterers ($M = 92$ in total) are inscribed at the inner sidewall. (b) Spontaneous emission spectrum of the quantum emitter under an external magnetic field from -9 T to 9 T (upper panel) versus the cavity resonance spectrum measured with a broadband input from a grating coupler and signal collection from the angular grating (lower panel). The comparison evidently shows, at $B = 6.0$ T or -6.0 T, the σ_+ or σ_- emission branch can be tuned on resonance, respectively, with the cavity mode centered at 767.9 nm (corresponding to the resonance order of $N = 99$) with a full width at half maximum (FWHM) of 0.1 nm. (c) Measured time-resolved photoluminescence spectra show a photon lifetime reduction from 30.3 to 16.0 ns when the quantum emitter is tuned from off-resonance (black) to on-resonance (red). (d) Second-order photon correlation histogram (blue dots) and its data fit (red curve) exhibit pronounced antibunching with $g^{(2)}(0) = 0.13 \pm 0.06$.

magnetic-tuned single-spin emission as a result of the valley Zeeman splitting where the positive (negative) magnetic field excites only valley pseudospin σ_+ (σ_-) at the K ($-$K) point in the Brillouin zone [27] [Fig. 2(b), upper panel]. The spectrum shows enhanced spontaneous emission under the magnetic field of $B = \pm 6.0$ T, which coincides with the microring resonance measured at the wavelength of 767.9 nm [Fig. 2(b), lower panel]. Time-resolved emission spectra further confirmed effective coupling between the quantum emitter and the cavity resonance, showing a reduction in the photon lifetime from 30.3 to 16 ns when the magnetic field is tuned from the off-resonance to on-resonance condition (i.e., $B = \pm 6.0$ T) [Fig. 2(c)]. This result corresponds to the Purcell enhancement of approximately $F_P \approx 2.5$–3.3, which, together with the measured lifetime decay, indicates an estimation of the off-resonance (on-resonance) quantum yield of the emitter to be $50 \pm 11\%$ ($76 \pm 6\%$) (see Supplemental Material [24]). The single photon purity was validated by characterizing the second-order correlation function $g^{(2)}(\tau)$ with the Hanbury Brown–Twiss interferometry, which displays pronounced single photon antibunching with $g^{(2)}(0) \sim 0.13 \pm 0.06$ [Fig. 2(d)].

To characterize the OAM signature of twisted single photons, the probability distribution of quantum light emission in the transverse dimension is captured in the far field by integrating many single photon events on an electron multiplying charge-coupled device camera. At the on-resonance condition of $B = \pm 6.0$ T, the combined use of a quarter wave plate and a linear polarizer helps selectively collect only the matching spin component (either σ_+ or σ_-). For example, at $B = 6.0$ T, only the σ_+ branch of the quantum emitter is activated to resonantly interact with the microring cavity. By residing at the outer sidewall, the quantum light emission can only couple to the TE-polarized CW mode according to the designed spin-orbit locking, which subsequently emits σ_--polarized single photons from the angular grating at the inner sidewall [Fig. 3(a)]. Because of the phase singularity at the center, the probability profile of twisted single photons with a nonzero topological charge l shows a doughnut shaped structure. Next, a computer-generated spiral phase hologram is implemented by a spatial light modulator and carries an opposite phase winding of $2\pi l'$. After the photons diffract from the phase hologram, the opposite phase winding modulates its transverse phase inversely, yielding a smaller doughnut shape with a topological charge of $l + l'$. If $l = -l'$, the phase singularity at the center is dissolved, as convincingly demonstrated by the observed on-axis bright spot. Here, the spot occurs under the modulation of the spiral phase hologram with $l' = -8$, experimentally confirming the topological charge of the generated twisted single photons: $l = 8$ consistent with the microring design ($l = N - M + 1$, where $N = 99$, $M = 92$) (see Supplemental Material [24]). As aforementioned, the magnetic switching to $B = -6.0$ T reverses all chiral signatures of the whole system [Fig. 3(b)]. While a similar doughnut shaped structure maintains in the far field, the polarization state of the twisted single photons becomes σ_+. Similar phase modulation also unambiguously showed convenient chiral switching of its topological charge to $l = -8$. It is worth noting that the magnetic field is high in the current experiment due to the relatively large frequency detuning between the cavity mode and the quantum emitter. However, strategical integration of on-chip thermal tuning [39] on the current Si_3N_4 platform is expected to reduce the cavity-emitter detuning and thus significantly lower the needed strength of the applied magnetic field.

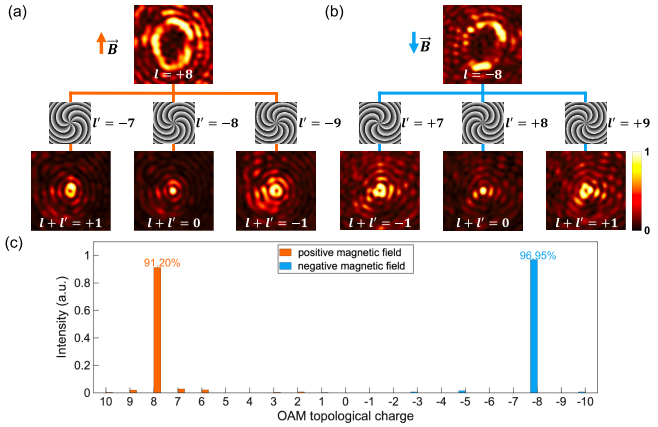

FIG. 3. High-purity generation and switching of twisted single photons. (a) Under a positive magnetic field, σ_--polarized far field radiation (top panel) receives transverse phase modulations by a series of spiral phase holograms with topological charges of $l' = -7$, -8, and -9 (middle panels), leading to shrunk doughnut shaped structures since phase modulations yield lower OAM orders of $l + l' = +1$, 0, and -1 (bottom panels), respectively. The occurrence of a bright spot at the center with the phase modulation of $l' = -8$ indicates that the OAM topological charge of the emitted single photons is $l = +8$. (b) When the magnetic field is switched negative, σ_+-polarized far-field radiation (top panel) receives transverse phase modulations with topological charges of $l' = +7$, $+8$, and $+9$ (middle panels), yielding lower OAM orders of $l + l' = -1$, 0, and $+1$ (bottom panels), respectively, which confirm the OAM topological charge of the emitted single photons $l = -8$. (c) The reconstructed histogram of OAM distribution based on measurement results shows high OAM purities of $91.20 \pm 0.03\%$ and $96.95 \pm 0.02\%$ for the generated twisted single photons under positive (orange) and negative (blue) magnetic fields, respectively. The uncertainty associated with the OAM purities is determined by considering the standard deviation of the background noise.

To precisely quantify the purity of the OAM state associated with the twisted single photons, we performed data postprocessing for mode decomposition using the maximum likelihood estimation. Experimentally captured images of far-field probability distribution maps of twisted single photons [top panels in Figs. 3(a) and 3(b)] are both decomposed into a series of Bessel modes with their OAM orders spanning from 10 to -10 by minimizing the error function (see Supplemental Material [24]). The decomposition results [Fig. 3(c)] clearly demonstrate a higher mode purity in our twisted single photon generation than previously reported using other integrated approaches [18,19]: $91.20 \pm 0.03\%$ and $96.95 \pm 0.02\%$ for $l = \pm 8$ at $B = \pm 6.0$ T, respectively. Note that the uncertainties in the mode purity above come mainly from the standard deviation of the background noise.

In addition to the high-purity generation and switching of twisted single photons, our platform also features effective on-chip chiral control and routing of quantum light in photonic integrated circuits. On-resonance coupling

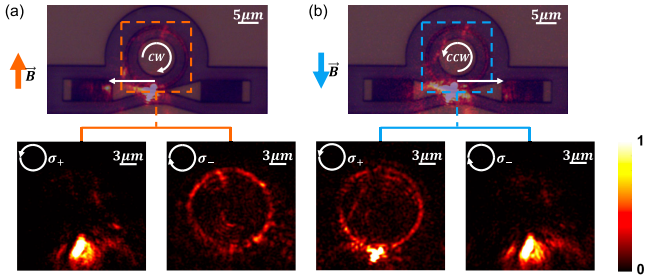

FIG. 4. Magnetically tuned single photon routing on-chip. (a), (b) Emission captured at the image plane of the device under positive and negative magnetic fields, respectively, where upper panels show the unpolarized image overlapped with the optical microscope picture of the device, and lower panels show the polarized emissions according to two photon spins. In (a), only the CW mode propagates in the microring, resulting in a strong output at the left grating coupler (upper). The result is consistent with the polarized emissions, as the CW mode carries opposite transverse spins of σ_+ at the outer sidewall and σ_- at the inner sidewall. Direct emission confirms the quantum emitter at the outer sidewall to be σ_+ polarized (lower left), which can couple into the CW mode and subsequently lead to the σ_--polarized ring-shaped emission from the angular grating at the inner sidewall (lower right). In (b), a strong output is observed at the right grating coupler, confirming the magnetic switching of the circulating mode to CCW and thus routing to the right direction in the bus waveguide (upper). Consequently, direct emission shows the quantum emitter to be σ_- polarized (lower right) and the ring-shaped emission is σ_+ polarized (lower left), consistent with excitation of the CCW mode that carries σ_- at the outer sidewall and σ_+ at the inner sidewall.

with a high-quality factor microring resonator facilitates a high β factor of approximately $47.2 \pm 4.1\%$ (see Supplemental Material [24]). When the 0D exciton in WSe_2 is formed at the quantum-chiral interface at the outer sidewall of the microring, single photons are forced to emit into only one circulating mode depending on the direction of the applied magnetic field. At $B = 6.0$ T, single photons emit into the CW mode, as evidently shown by strong output from the left grating coupler [Fig. 4(a)]. Note that at the image plane, both spin components (σ_+ and σ_-) are collected, corresponding to photons directly emitted from the quantum emitter and photons coupled into the microring, respectively. Similarly, the spin-orbit chiral control forces the single photon emission into the CCW mode by switching the magnetic field to $B = -6.0$ T, effectively routing quantum light to the right grating coupler [Fig. 4(b)]. For applications in on-chip quantum information processing, the angular grating inscribed on the inner sidewall of the microring becomes unnecessary. Its removal can significantly increase the quality factor of the microring and thus enhance the emitter-cavity coupling. In this regard, the chiral selectivity of our device may enable efficient single photon isolation [40], creating a quantum photonic diode—a fundamental building block toward large-scale quantum photonic systems.

The high-purity generation and switching of twisted single photons we have accomplished using integrated photonics is expected to have strong impacts in both fundamental physics and device applications. The ability to manipulate OAM at the single photon level can enable quantum information encoding and transmission using the free space spin-orbit modes, which can potentially achieve high-dimensional qudits for drastic expansion of quantum information capacity and enhancement of communication security, even without the requirement of photon indistinguishability [41,42]. Although the realization of a high photon indistinguishability remains challenging for most solid-state single photon sources [42,43], especially for WSe_2 quantum emitters, strategical engineering of a resonant system with a large Purcell factor, for example, hybrid integration of a plasmonic nanocavity with the quantum emitter, can potentially address this issue by shortening the emitter lifetime to enforce the quantum emitter working in the coherence regime [44]. The flexible quantum emitter creation process makes our scheme easily adapted to other integrated photonic platforms, such as $LiNbO_3$ on insulator platform, where the frequency tuning via the strong electro-optical effect can not only decrease the required magnetic field, but also provides the potential for ultrafast modulation of the topological charge of the single photons [45]. The performed chiral control of light-matter interaction in the quantum regime can facilitate a series of intriguing quantum functionalities such as on-chip routing and isolation needed for the deployment of integrated quantum photonics. Moreover, switching to the recently developed room-temperature deterministically created quantum emitter in monolayer *h*-BN provides the opportunity to operate our device at room temperature [46], thus improving its scalability for quantum applications.

We acknowledge financial support from the National Science Foundation (ECCS-Raise-EQuIP-1842612, ECCS-1932803, ECCS-MRI-1531237, NNCI-1542153, DMR-1420634). Fabrication work was carried out in part at the Singh Center for Nanotechnology, which is supported by the NSF National Nanotechnology Coordinated Infrastructure. Materials synthesis was supported by the NSF MRSEC program through Columbia in the Center for Precision Assembly of Superstratic and Superatomic Solids.

*These authors contributed equally to this work.
†strauf@stevens.edu
‡fenglia@seas.upenn.edu

[1] S.-K. Liao *et al.*, Nature (London) **549**, 43 (2017).
[2] M. Bloch, S. W. McLaughlin, J.-M. Merolla, and F. Patois, Opt. Lett. **32**, 301 (2007).
[3] J. M. Donohue, M. Agnew, J. Lavoie, and K. J. Resch, Phys. Rev. Lett. **111**, 153602 (2013).
[4] J. Wang *et al.*, Science **360**, 285 (2018).
[5] L. Allen, M. W. Beijersbergen, R. J. C. Spreeuw, and J. P. Woerdman, Phys. Rev. A **45**, 8185 (1992).
[6] M. Erhard, R. Fickler, M. Krenn, and A. Zeilinger, Light Sci. Appl. **7**, 17146 (2018).
[7] M. Mafu, A. Dudley, S. Goyal, D. Giovannini, M. McLaren, M. J. Padgett, T. Konrad, F. Petruccione, N. Lütkenhaus, and A. Forbes, Phys. Rev. A **88**, 032305 (2013).
[8] B. Bahari, L. Hsu, S. H. Pan, D. Preece, A. Ndao, A. El Amili, Y. Fainman, and B. Kanté, Nat. Phys. **17**, 700 (2021).
[9] P. Miao, Z. Zhang, J. Sun, W. Walasik, S. Longhi, N. M. Litchinitser, and L. Feng, Science **353**, 464 (2016).
[10] A. Sit *et al.*, Optica **4**, 1006 (2017).
[11] N. J. Cerf, M. Bourennane, A. Karlsson, and N. Gisin, Phys. Rev. Lett. **88**, 127902 (2002).
[12] A. Mair, A. Vaziri, G. Weihs, and A. Zeilinger, Nature (London) **412**, 313 (2001).
[13] X.-L. Wang, X.-D. Cai, Z.-E. Su, M.-C. Chen, D. Wu, L. Li, N.-L. Liu, C.-Y. Lu, and J.-W. Pan, Nature (London) **518**, 516 (2015).
[14] R. Fickler, R. Lapkiewicz, W. N. Plick, M. Krenn, C. Schaeff, S. Ramelow, and A. Zeilinger, Science **338**, 640 (2012).
[15] T. Stav, A. Faerman, E. Maguid, D. Oren, V. Kleiner, E. Hasman, and M. Segev, Science **361**, 1101 (2018).
[16] I. Aharonovich, D. Englund, and M. Toth, Nat. Photonics **10**, 631 (2016).
[17] J. Ni, C. Huang, L.-M. Zhou, M. Gu, Q. Song, Y. Kivshar, and C.-W. Qiu, Science **374**, eabj0039 (2021).
[18] B. Chen, Y. Wei, T. Zhao, S. Liu, R. Su, B. Yao, Y. Yu, J. Liu, and X. Wang, Nat. Nanotechnol. **16**, 302 (2021).
[19] C. Wu, S. Kumar, Y. Kan, D. Komisar, Z. Wang, S. I. Bozhevolnyi, and F. Ding, Sci. Adv. **8**, eabk3075 (2022).
[20] D. Komisar, S. Kumar, Y. Kan, C. Wu, and S. I. Bozhevolnyi, ACS Photonics **8**, 2190 (2021).
[21] Z. Zhang *et al.*, Science **368**, 760 (2020).
[22] Z. Zhang, H. Zhao, D. G. Pires, X. Qiao, Z. Gao, J. M. Jornet, S. Longhi, N. M. Litchinitser, and L. Feng, Light Sci. Appl. **9**, 179 (2020).
[23] Z. Shao, J. Zhu, Y. Chen, Y. Zhang, and S. Yu, Nat. Commun. **9**, 926 (2018).
[24] See Supplemental Material at http://link.aps.org/supplemental/10.1103/PhysRevLett.131.183801 for details, which includes Refs. [25–31].
[25] A. Srivastava, M. Sidler, A. V. Allain, D. S. Lembke, A. Kis, and A. Imamoğlu, Nat. Nanotechnol. **10**, 491 (2015).
[26] L. Linhart, M. Paur, V. Smejkal, J. Burgdörfer, T. Mueller, and F. Libisch, Phys. Rev. Lett. **123**, 146401 (2019).
[27] Y. Ma, H. Zhao, N. Liu, Z. Gao, S. S. Mohajerani, L. Xiao, J. Hone, L. Feng, and S. Strauf, Optica **9**, 953 (2022).
[28] G. D. Shepard, O. A. Ajayi, X. Li, X. Zhu, J. Hone, and S. Strauf, 2D Mater. **4**, 021019 (2017).
[29] D. Edelberg *et al.*, Nano Lett. **19**, 4371 (2019).
[30] L. Peng, H. Chan, P. Choo, T. W. Odom, S. K. Sankaranarayanan, and X. Ma, Nano Lett. **20**, 5866 (2020).
[31] Y. Luo, G. D. Shepard, J. V. Ardelean, D. A. Rhodes, B. Kim, K. Barmak, J. C. Hone, and S. Strauf, Nat. Nanotechnol. **13**, 1137 (2018).
[32] P. Lodahl, S. Mahmoodian, S. Stobbe, A. Rauschenbeutel, P. Schneeweiss, J. Volz, H. Pichler, and P. Zoller, Nature (London) **541**, 473 (2017).

[33] L. Sapienza, M. Davanço, A. Badolato, and K. Srinivasan, Nat. Commun. **6**, 7833 (2015).
[34] S. I. Azzam, K. Parto, and G. Moody, Appl. Phys. Lett. **118** (2021).
[35] M. Turunen, M. Brotons-Gisbert, Y. Dai, Y. Wang, E. Scerri, C. Bonato, K. D. Jöns, Z. Sun, and B. D. Gerardot, Nat. Rev. Phys. **4**, 219 (2022).
[36] F. Peyskens, C. Chakraborty, M. Muneeb, D. Van Thourhout, and D. Englund, Nat. Commun. **10**, 4435 (2019).
[37] M. Blauth, M. Jurgensen, G. Vest, O. Hartwig, M. Prechtl, J. Cerne, J. J. Finley, and M. Kaniber, Nano Lett. **18**, 6812 (2018).
[38] J. Zhu, X. Cai, Y. Chen, and S. Yu, Opt. Lett. **38**, 1343 (2013).
[39] Y. Luo, N. Liu, X. Li, J. C. Hone, and S. Strauf, 2D Mater. **6**, 035017 (2019).
[40] C. Sayrin, C. Junge, R. Mitsch, B. Albrecht, D. O'Shea, P. Schneeweiss, J. Volz, and A. Rauschenbeutel, Phys. Rev. X **5**, 041036 (2015).
[41] T. Gao, M. von Helversen, C. Antón-Solanas, C. Schneider, and T. Heindel, npj 2D Mater. Appl. **7**, 4 (2023).
[42] I. Aharonovich, D. Englund, and M. Toth, Nat. Photonics **10**, 631 (2016).
[43] A. V. Kuhlmann, J. Houel, A. Ludwig, L. Greuter, D. Reuter, A. D. Wieck, M. Poggio, and R. J. Warburton, Nat. Phys. **9**, 570 (2013).
[44] Y. Luo, X. He, Y. Kim, J. L. Blackburn, S. K. Doorn, H. Htoon, and S. Strauf, Nano Lett. **19**, 9037 (2019).
[45] C. Wang, M. Zhang, X. Chen, M. Bertrand, A. Shams-Ansari, S. Chandrasekhar, P. Winzer, and M. Lončar, Nature (London) **562**, 101 (2018).
[46] I. Aharonovich, J.-P. Tetienne, and M. Toth, Nano Lett. **22**, 9227 (2022).